Article

Structure of M^{pro} from SARS-CoV-2 and discovery of its inhibitors

https://doi.org/10.1038/s41586-020-2223-y

Received: 9 February 2020

Accepted: 1 April 2020

Published online: 9 April 2020

Check for updates

Zhenming Jin[1,2,10], Xiaoyu Du[2,10], Yechun Xu[3,10], Yongqiang Deng[4,10], Meiqin Liu[5,10], Yao Zhao[1], Bing Zhang[1], Xiaofeng Li[4], Leike Zhang[5], Chao Peng[6], Yinkai Duan[1], Jing Yu[1], Lin Wang[1], Kailin Yang[7], Fengjiang Liu[1], Rendi Jiang[5], Xinglou Yang[5], Tian You[1], Xiaoce Liu[1], Xiuna Yang[1], Fang Bai[1], Hong Liu[3], Xiang Liu[8], Luke W. Guddat[9], Wenqing Xu[1,6], Gengfu Xiao[5], Chengfeng Qin[4], Zhengli Shi[5], Hualiang Jiang[1,3]✉, Zihe Rao[1,2,8]✉ & Haitao Yang[1]✉

A new coronavirus, known as severe acute respiratory syndrome coronavirus 2 (SARS-CoV-2), is the aetiological agent responsible for the 2019–2020 viral pneumonia outbreak of coronavirus disease 2019 (COVID-19)[1–4]. Currently, there are no targeted therapeutic agents for the treatment of this disease, and effective treatment options remain very limited. Here we describe the results of a programme that aimed to rapidly discover lead compounds for clinical use, by combining structure-assisted drug design, virtual drug screening and high-throughput screening. This programme focused on identifying drug leads that target main protease (M^{pro}) of SARS-CoV-2: M^{pro} is a key enzyme of coronaviruses and has a pivotal role in mediating viral replication and transcription, making it an attractive drug target for SARS-CoV-2[5,6]. We identified a mechanism-based inhibitor (N3) by computer-aided drug design, and then determined the crystal structure of M^{pro} of SARS-CoV-2 in complex with this compound. Through a combination of structure-based virtual and high-throughput screening, we assayed more than 10,000 compounds—including approved drugs, drug candidates in clinical trials and other pharmacologically active compounds—as inhibitors of M^{pro}. Six of these compounds inhibited M^{pro}, showing half-maximal inhibitory concentration values that ranged from 0.67 to 21.4 μM. One of these compounds (ebselen) also exhibited promising antiviral activity in cell-based assays. Our results demonstrate the efficacy of our screening strategy, which can lead to the rapid discovery of drug leads with clinical potential in response to new infectious diseases for which no specific drugs or vaccines are available.

Coronaviruses infect humans and other animals and cause a variety of highly prevalent and severe diseases, including severe acute respiratory syndrome (SARS) and Middle East respiratory syndrome (MERS)[7]. The SARS-CoV-2 genome comprises about 30,000 nucleotides: the replicase gene of SARS-CoV-2 encodes two overlapping polyproteins—pp1a and pp1ab—that are required for viral replication and transcription[3,4]. The functional polypeptides are released from the polyproteins by extensive proteolytic processing, predominantly by the 33.8-kDa M^{pro} (also known as 3C-like protease). M^{pro} digests the polyprotein at at least 11 conserved sites, starting with the autolytic cleavage of this enzyme itself from pp1a and pp1ab[8]. The functional importance of M^{pro} in the viral life cycle, combined with the absence of closely related homologues in humans, identify M^{pro} as an attractive target for the design of antiviral drugs[9].

To facilitate the rapid discovery of antiviral compounds with clinical potential, we developed a strategy that combines structure-assisted drug design, virtual drug screening and high-throughput screening to repurpose existing drugs to target SARS-CoV-2 M^{pro}.

Establishing a high-throughput activity assay

Recombinant SARS-CoV-2 M^{pro} with native N and C termini was expressed in *Escherichia coli*, and subsequently purified (Extended Data Fig. 1a, b). The molecular mass of SARS-CoV-2 M^{pro} as determined

[1]Shanghai Institute for Advanced Immunochemical Studies and School of Life Science and Technology, ShanghaiTech University, Shanghai, China. [2]Laboratory of Structural Biology, School of Life Sciences and School of Medicine, Tsinghua University, Beijing, China. [3]Drug Discovery and Design Center, Shanghai Institute of Materia Medica, Chinese Academy of Sciences, Shanghai, China. [4]Department of Virology, State Key Laboratory of Pathogen and Biosecurity, Beijing Institute of Microbiology and Epidemiology, Academy of Military Medical Sciences, Beijing, China. [5]CAS Key Laboratory of Special Pathogens, Wuhan Institute of Virology, Center for Biosafety Mega-Science, Chinese Academy of Sciences, Wuhan, China. [6]National Facility for Protein Science in Shanghai, Zhangjiang Lab, Shanghai Advanced Research Institute, Chinese Academy of Science, Shanghai, China. [7]Taussig Cancer Center, Cleveland Clinic, Cleveland, OH, USA. [8]State Key Laboratory of Medicinal Chemical Biology, Frontiers Science Center for Cell Response, College of Life Sciences, College of Pharmacy, Nankai University, Tianjin, China. [9]School of Chemistry and Molecular Biosciences, the University of Queensland, Brisbane, Queensland, Australia. [10]These authors contributed equally: Zhenming Jin, Xiaoyu Du, Yechun Xu, Yongqiang Deng, Meiqin Liu. ✉e-mail: hljiang@simm.ac.cn; raozh@mail.tsinghua.edu.cn; yanght@shanghaitech.edu.cn

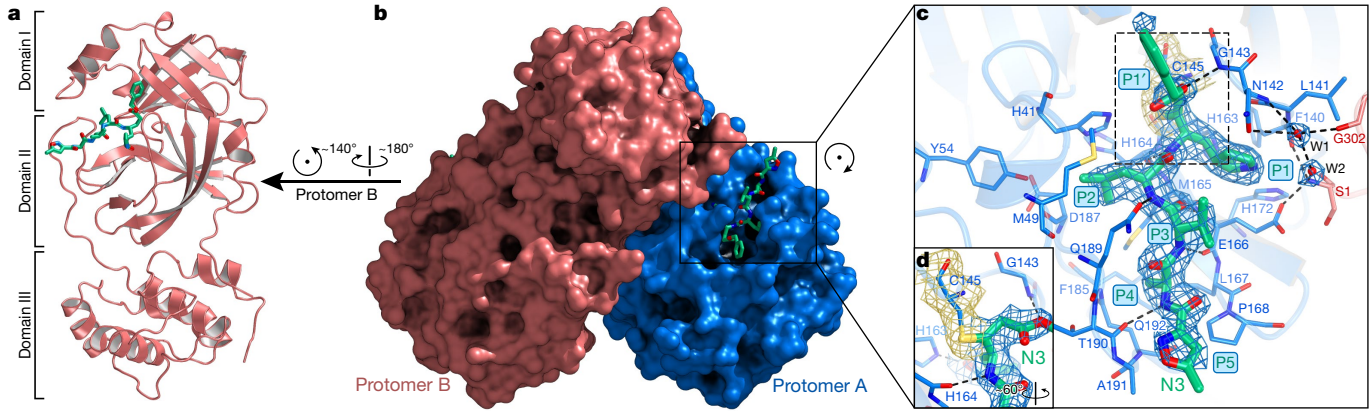

Fig. 1 | The crystal structure of SARS-CoV-2 M^{pro} in complex with N3. **a**, Cartoon representation of one protomer of the dimeric M^{pro}–inhibitor complex. **b**, Surface representation of the homodimer of M^{pro}. Protomer A is in blue, protomer B is in salmon, N3 is presented as green sticks. **c**, An enlarged view of the substrate-binding pocket. The key residues that form the binding pocket are shown in sticks; the two water molecules (W1 and W2) are shown as red spheres. The P1, P1′, P2, P3, P4 and P5 sites of N3 are indicated. Hydrogen bonds that help to lock the inhibitor are shown in black dashed lines. The $2F_o - F_c$ density map contoured at 1.2σ is shown around N3 molecule (blue mesh), C145 of protomer A (yellow mesh) and the two waters (blue mesh). **d**, The C–S covalent bond.

by mass spectroscopy is 33797.0 Da, consistent with its theoretical molecular mass of 33796.8 Da. To characterize the enzymatic activity of SARS-CoV-2 M^{pro} and to carry out high-throughput screening of inhibitors, we developed a fluorescence resonance energy transfer assay. To do this, we designed and synthesized the fluorescently labelled substrate Mca–AVLQ↓SGFRK(Dnp)K, derived from the N-terminal autocleavage sequence of the viral protease, for time-dependent kinetic analysis (Extended Data Fig. 1e). The catalytic efficiency (k_{cat}/K_m) for SARS-CoV-2 M^{pro} was measured to be 28,500 $M^{-1}\,s^{-1}$, which is slightly higher than that for SARS-CoV M^{pro} (k_{cat}/K_m = 26,500 $M^{-1}\,s^{-1}$)[10] and more than 30-fold higher than that of human rhinovirus 3C protease (k_{cat}/K_m = 920 $M^{-1}s^{-1}$)[11].

N3 is a potent inhibitor of SARS-CoV-2 M^{pro}

In a previous study[12], a Michael acceptor inhibitor—known as N3—was developed using computer-aided drug design (Extended Data Fig. 1c). N3 can specifically inhibit M^{pro} from multiple coronaviruses, including SARS-CoV and MERS-CoV[12–15], and has displayed potent antiviral activity against infectious bronchitis virus in an animal model[13]. The 50% cytotoxicity concentration of N3 is >133 μM (Extended Data Fig. 1f). Next, we constructed a homology model for SARS-CoV-2 M^{pro}, and used molecular docking to see whether N3 could target this M^{pro}. A docking pose showed that N3 could fit inside the substrate-binding pocket. To assess the efficacy of N3 for SARS-CoV-2 M^{pro}, we performed kinetic analysis. A progress curve showed that it is a time-dependent irreversible inhibitor of this enzyme. Further, the shape of this curve supports the mechanism of two-step irreversible inactivation. The inhibitor first associates with SARS-CoV-2 M^{pro} with a dissociation constant K_i, and then a stable covalent bond is formed between N3 and M^{pro}. The evaluation of this time-dependent inhibition requires both the equilibrium-binding constant (K_i, designated as k_2/k_1) and the inactivation-rate constant for covalent bond formation, k_3. However, N3 exhibits a very potent inhibition of SARS-CoV-2 M^{pro}, such that the measurement of K_i and k_3 was not feasible (Extended Data Fig. 1d, e). When very rapid inactivation occurs, $k_{obs}/[I]$ was used to evaluate the inhibition as an approximation of the pseudo-second-order rate constant (k_3/K_i)[12]. We determined the value of $k_{obs}/[I]$ of N3 for SARS-CoV-2 M^{pro} as 11,300 ± 880 $M^{-1}\,s^{-1}$, which suggests that this Michael acceptor was markedly inhibited.

Crystal structure of SARS-CoV-2 M^{pro}–N3

To elucidate the inhibitory mechanism of N3, we determined the crystal structure of SARS-CoV-2 M^{pro} in complex with N3 to a resolution of 2.1 Å. The asymmetric unit contains only one polypeptide (Extended Data Table 1). However, two of these polypeptides (designated protomer A and B) associate to form a dimer by a crystallographic two-fold axis of symmetry (Fig. 1b). All of the residues 1–306 are visible in electron density maps. Each protomer is composed of three domains (Fig. 1a). Domain I (residues 8–101) and domain II (residues 102–184) have an antiparallel β-barrel structure. Domain III (residues 201–303) contains five α-helices arranged into a largely antiparallel globular cluster, and it is connected to domain II by a long loop region (residues 185–200). SARS-CoV-2 M^{pro} has a Cys-His catalytic dyad, and the substrate-binding site is located in a cleft between domain I and domain II. These features are similar to previously reported M^{pro} from other coronaviruses[5,6,13–15]. The electron density map shows that N3 binds in the substrate-binding pocket in an extended conformation (Fig. 1c, Extended Data Fig. 2); the inhibitor backbone atoms form an antiparallel sheet with residues 164–168 of the long strand (residues 155–168) on one side, and with residues 189–191 of the loop that links domain II to domain III on the other.

Here we detail the specific interactions of N3 with M^{pro} (Fig. 1c, d). The electron density shows that the Sγ atom of C145 of protomer A forms a covalent bond (1.8 Å) with the Cβ atom of the vinyl group, confirming that the Michael addition has occurred. The S1 subsite has an absolute requirement for Gln at the P1 position. The side chains of F140, N142, E166, H163 and H172 of protomer A, and S1 of protomer B—as well as the main chains of F140 and L141 of protomer A—are involved in the formation of the S1 subsite, which also includes two ordered water molecules (which we refer to as W1 and W2). The lactam at P1 inserts into the S1 subsite and forms a hydrogen bond with H163 of protomer A. The side chain of Leu at the P2 site inserts deeply into the hydrophobic S2 subsite, which consists of the side chains of H41, M49, Y54 and M165, as well as the alkyl portion of the side chain of D187, of protomer A. The side chain of Val at P3 is solvent-exposed, which indicates that this site can tolerate a wide range of functional groups. The side chain of Ala at the P4 side is surrounded by the side chains of M165, L167, F185, Q192 of protomer A and the main chain of Q189 of protomer A, which together form a small hydrophobic pocket. P5 makes van der Waals contacts with P168 of protomer A, and with the backbone of

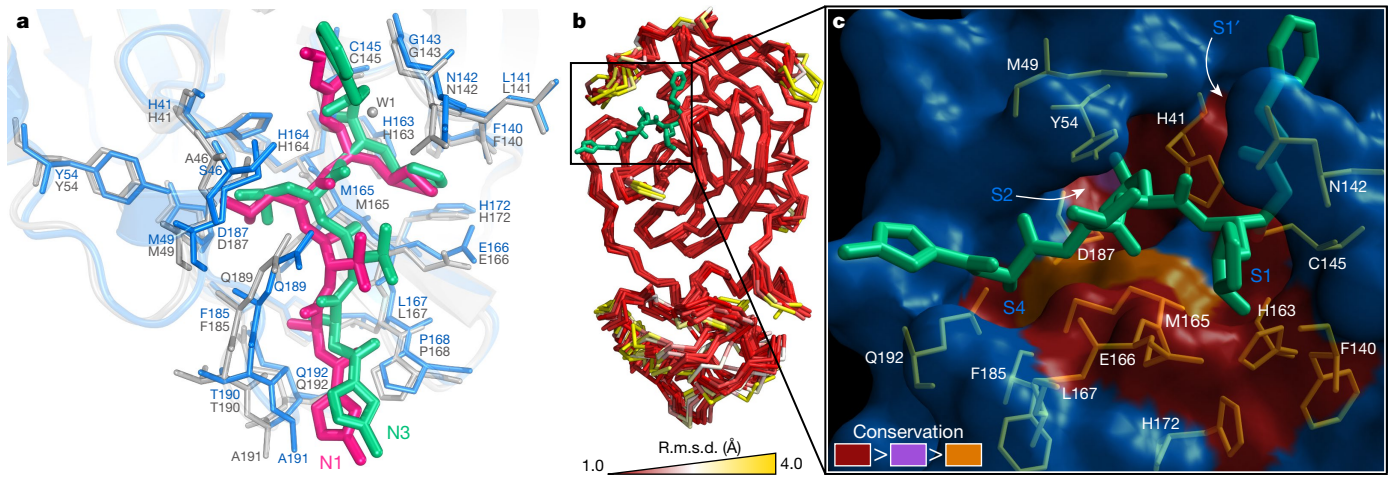

Fig. 2 | The substrate-binding pockets of M^{pro} across different species of coronavirus. a, Comparison of inhibitor binding mode between the structures of SARS-CoV-2 M^{pro}–N3 and SARS-CoV M^{pro}–N1. SARS-CoV-2 M^{pro} is shown in marine cartoon; SARS-CoV M^{pro} in grey; N3 in green sticks; and N1 in hot pink. **b**, Superposition of crystal structures of M^{pro} (Cα 1–300) from 12 coronaviruses, including SARS-CoV-2, SARS-CoV, MERS-CoV, human coronavirus (HCoV)-HKU1, bat coronavirus HKU4, mouse hepatitis virus A59, porcine epidemic diarrhoea virus, feline infectious peritonitis virus, transmissible gastroenteritis virus, HCoV-NL63, HCoV-229E and infectious bronchitis virus. The colour spectrum represents the root-mean-square deviation (r.m.s.d.) of the aligned Cα atoms. **c**, Surface presentation of conserved substrate-binding pockets of M^{pro} from 12 coronaviruses. Red, residues are entirely identical among M^{pro} in all 12 viruses; violet, conserved substitution in M^{pro} of one of the coronaviruses; orange, conserved substitution in M^{pro} of more than one of the coronaviruses. S1, S2, S4 and S1′ subsites are indicated.

residues 190–191. The bulky benzyl group extends into the S1′ site, forming van der Waals interactions with T24 and T25 of protomer A. N3 forms multiple hydrogen bonds with the main chain of the residues in the substrate-binding pocket, which also helps to lock the inhibitor inside the substrate-binding pocket.

An overlay of the structures of SARS-CoV-2 M^{pro} in complex with N3 and SARS-CoV M^{pro} in complex with N1 (ref. [12]), an alternative Michael acceptor inhibitor, shows that N3 and N1 bind to M^{pro} in a similar mode (Fig. 2a, Extended Data Fig. 3). The major difference lies in the P1′ site. Compared with the benzyl ester portion of N3 in the SARS-CoV-2 M^{pro}–N3 structure, the ethyl ester portion in N1 in SARS-CoV M^{pro}–N1 adopts a slightly different conformation. This can be attributed to an ordered water (W1) in the SARS-CoV M^{pro}–N1 structure, which makes a long-distance hydrogen bond to the carboxylate oxygen of the ester and also forms two hydrogen bonds from the backbone NH of G143 and the side chain of N142. A previous study proposed that M^{pro} has substrate-recognition pocket that is highly conserved among all coronaviruses, and that this pocket could serve as a drug target for the design of broad-spectrum inhibitors[12]. The recent discovery of new coronaviruses, and the accumulation of structural data for M^{pro} from coronaviruses of various species, provided the opportunity to further examine this hypothesis. Superposition of the 12 crystal structures of M^{pro} (refs. [12–21]) shows that the most variable regions are the helical domain III and surface loops, and that the substrate-binding pocket (located in a cleft between domain I and domain II) is highly conserved among M^{pro} in all coronaviruses; this suggests that antiviral inhibitors targeting this pocket should have wide-spectrum activity against coronaviruses (Fig. 2b, c).

Virtual screening

The structure of SARS-CoV-2 M^{pro} in complex with N3 provides a model for identifying lead inhibitors to target SARS-CoV-2 M^{pro} using in silico screening. To achieve this, we docked an in-house database of potential binding compounds using Glide (v.8.2)[22]. The results show that cinanserin fits snugly into the substrate-binding pocket, through cation–π interactions with H41 and E166 of M^{pro}. Subsequently, we determined this compound has a half-maximal inhibitory concentration (IC_{50}) value of 125 μM for M^{pro}. Moreover, cinanserin is a well-characterized serotonin antagonist, which underwent preliminary clinical testing in humans in the 1960s[23] and has previously been shown to inhibit SARS-CoV M^{pro} (ref. [24]). The 50% cytotoxicity concentration of cinanserin is >200 μM (Extended Data Fig. 4); thus, it has potential for optimization as an antiviral drug lead.

High-throughput screening

Next, we used our fluorescence resonance energy transfer assay to screen a library of about 10,000 compounds, consisting of approved drugs, clinical-trial drug candidates and natural products. The primary hits were seven compounds, including approved drugs (disulfiram and carmofur) as well as preclinical or clinical-trial drug candidates (ebselen, shikonin, tideglusib, PX-12 and TDZD-8). We then determined the IC_{50} values of these seven compounds, which range from 0.67 to 21.4 μM (Fig. 3). Ebselen has the strongest inhibition of M^{pro} activity, with an IC_{50} of 0.67 μM. Using a previously described detergent-based assay[25], we found that TDZD-8 is an aggregate-based inhibitor that might nonspecifically inhibit M^{pro} (Extended Data Fig. 5); it was, therefore, not considered for further investigation. Next, we set out to identify the potential covalent inhibitors among these compounds through tandem mass spectrometry analysis. The tandem mass spectrometry data show that ebselen, PX-12 and carmofur are all able to covalently bind to C145 of the catalytic dyad in SARS-CoV-2 M^{pro}. However, PX-12 and carmofur completely modified M^{pro}, whereas ebselen could only partially modify this cysteine of the viral protease (Extended Data Fig. 6). As ebselen has a stronger inhibitory effect than the other compounds, there is a possibility that ebselen could also inhibit M^{pro} through noncovalent binding. It is likely that a portion of the hits identified by screening are covalently bonded to the catalytic cysteine of M^{pro} through their sulfhydryl groups. In general, such molecules are expected to be promiscuous binders and therefore—as they stand—may have limited potential as drug leads. As our structural data are based on N3, we investigated whether molecular docking could predict how disulfiram, tideglusib and shikonin bind to

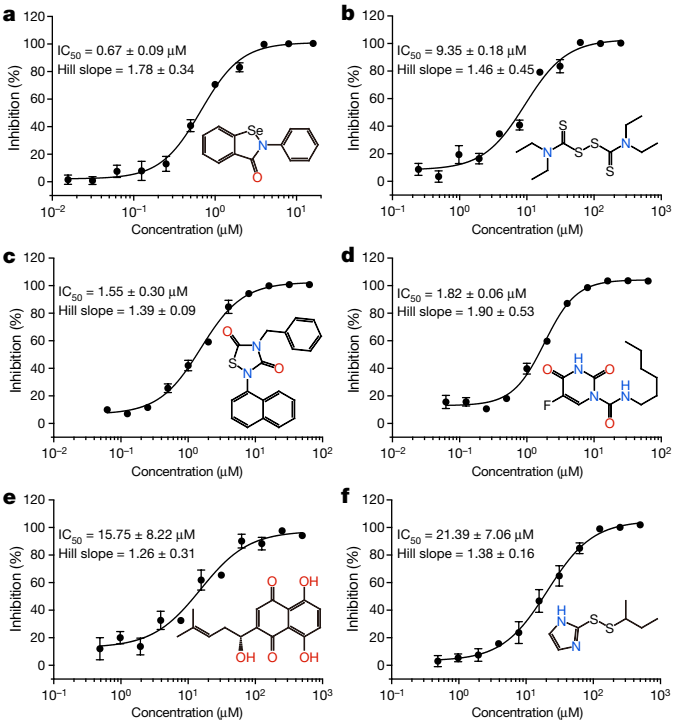

Fig. 3 | Drug leads inhibit the activity of SARS-CoV-2 M^{pro}. a–f, The hydrolytic activity of SARS-CoV-2 M^{pro} was measured in the presence of increasing concentrations of the drug candidates. **a**, Ebselen. **b**, Disulfiram. **c**, Tideglusib. **d**, Carmofur. **e**, Shikonin. **f**, PX-12. Dose–response curves for IC_{50} values were determined by nonlinear regression. All data are shown as mean ± s.e.m., $n = 3$ biological replicates.

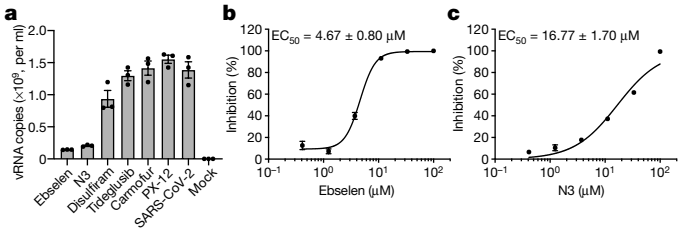

Fig. 4 | Antiviral activities of the drug leads against SARS-CoV-2. a, The quantification of absolute viral RNA (vRNA) copies (per ml) in the supernatant at 72 h after infection, determined by qRT–PCR analysis. Data are mean ± s.e.m., $n = 3$ biological replicates. **b**, **c**, Dose–response curves for ebselen (**b**) and N3 (**c**) in the plaque-reduction assay. All data are shown as mean ± s.e.m., $n = 4$ biological replicates.

this protein. In all cases, reasonable docking poses were found, which demonstrates that they could fit inside the substrate-binding pocket (Extended Data Fig. 7).

Antiviral activity assay

To further substantiate the enzymatic inhibition results in vitro, we evaluated whether these compounds could prevent viral replication in cell-based assays. As shown in Fig. 4a, quantitative real-time RT–PCR (qRT–PCR) demonstrated that, among these compounds, ebselen and N3 showed the strongest antiviral effects at a concentration of 10 μM treatment in SARS-CoV-2-infected Vero cells. We performed a plaque-reduction assay (Extended Data Fig. 8) to further assess the efficacy of these two compounds in protecting cells. Ebselen and N3 displayed inhibition against SARS-CoV-2 with individual half-maximal effective concentration (EC_{50}) values of 4.67 μM and 16.77 μM, respectively (Fig. 4b, c). The dose–response curves suggest that both of these compounds may be able to penetrate the cellular membrane to access their targets. Ebselen is an organoselenium compound with anti-inflammatory, anti-oxidant and cytoprotective properties. This compound has previously been investigated for the treatment of multiple diseases, including bipolar disorders[26] and hearing loss[27,28]. Ebselen has extremely low cytotoxicity (the median lethal dose in rats is >4,600 mg kg^{-1}, when taken orally)[29], and its safety in humans has been evaluated in a number of clinical trials[27,28,30]. These data strongly suggest the clinical potential of ebselen for the treatment of coronaviruses. It is also interesting to note that cinanserin displayed moderate inhibition against SARS-CoV-2 with an EC_{50} value of 20.61 μM, as shown from qRT–PCR analysis (Extended Data Fig. 4). This value is superior to that in the enzymatic inhibition assay, which suggests that cinanserin might have multidrug targets in preventing viral infection. In further studies, the selection and characterization of drug-resistant mutants will help to clarify the mode of action of cinanserin.

Discussion

Our crystal structural and docking data show that the drug leads we identified can bind to the substrate-binding pocket of SARS-CoV-2 M^{pro}, which is highly conserved among all coronaviruses. This strongly supports our hypothesis that the development of a single antiviral agent targeting M^{pro}, or such an agent used in combination with other potential therapies, could provide an effective first line of defence against all diseases associated with coronaviruses.

In the last 20 years, new infectious agents—such as SARS and MERS—have emerged and caused epidemics[7]. The timely development of effective antiviral agents for clinical use is extremely challenging, because conventional drug development approaches normally take years of investigation and cost billions of dollars. The repurposing of approved pharmaceutical drugs and drug candidates provides an alternative approach that allows for the rapid identification of potential drug leads to manage rapidly emerging viral infections. Cell-based phenotypic screening has proven to be valuable[31], but the complexity of this approach is not readily compatible with high-throughput pipelines, and it cannot identify the molecular target or mechanism of action[32]. In this study, the convergence of structure-based ab initio drug design, virtual screening and high-throughput screening proved to be an efficient strategy to find antiviral leads against SARS-CoV-2. The methods presented here can greatly assist in the rapid discovery of drug leads with clinical potential in response to new emerging infectious diseases that currently lack specific drugs and vaccines.

Online content

Any methods, additional references, Nature Research reporting summaries, source data, extended data, supplementary information, acknowledgements, peer review information; details of author contributions and competing interests; and statements of data and code availability are available at https://doi.org/10.1038/s41586-020-2223-y.

1. Zhu, N. et al. A novel coronavirus from patients with pneumonia in China, 2019. *N. Engl. J. Med.* **382**, 727–733 (2020).
2. Li, Q. et al. Early transmission dynamics in Wuhan, China, of novel coronavirus-infected pneumonia. *N. Engl. J. Med.* **382**, 1199–1207 (2020).
3. Zhou, P. et al. A pneumonia outbreak associated with a new coronavirus of probable bat origin. *Nature* **579**, 270–273 (2020).
4. Wu, F. et al. A new coronavirus associated with human respiratory disease in China. *Nature* **579**, 265–269 (2020).
5. Anand, K. et al. Structure of coronavirus main proteinase reveals combination of a chymotrypsin fold with an extra α-helical domain. *EMBO J.* **21**, 3213–3224 (2002).
6. Yang, H. et al. The crystal structures of severe acute respiratory syndrome virus main protease and its complex with an inhibitor. *Proc. Natl Acad. Sci. USA* **100**, 13190–13195 (2003).

7. de Wit, E., van Doremalen, N., Falzarano, D. & Munster, V. J. SARS and MERS: recent insights into emerging coronaviruses. *Nat. Rev. Microbiol*. **14**, 523–534 (2016).
8. Hegyi, A. & Ziebuhr, J. Conservation of substrate specificities among coronavirus main proteases. *J. Gen. Virol*. **83**, 595–599 (2002).
9. Pillaiyar, T., Manickam, M., Namasivayam, V., Hayashi, Y. & Jung, S. H. An overview of severe acute respiratory syndrome-coronavirus (SARS-CoV) 3CL protease inhibitors: peptidomimetics and small molecule chemotherapy. *J. Med. Chem*. **59**, 6595–6628 (2016).
10. Xue, X. et al. Production of authentic SARS-CoV M^{pro} with enhanced activity: application as a novel tag-cleavage endopeptidase for protein overproduction. *J. Mol. Biol*. **366**, 965–975 (2007).
11. Wang, Q. M., Johnson, R. B., Cox, G. A., Villarreal, E. C. & Loncharich, R. J. A continuous colorimetric assay for rhinovirus-14 3C protease using peptide *p*-nitroanilides as substrates. *Anal. Biochem*. **252**, 238–245 (1997).
12. Yang, H. et al. Design of wide-spectrum inhibitors targeting coronavirus main proteases. *PLoS Biol*. **3**, e324 (2005).
13. Xue, X. et al. Structures of two coronavirus main proteases: implications for substrate binding and antiviral drug design. *J. Virol*. **82**, 2515–2527 (2008).
14. Ren, Z. et al. The newly emerged SARS-like coronavirus HCoV-EMC also has an "Achilles' heel": current effective inhibitor targeting a 3C-like protease. *Protein Cell* **4**, 248–250 (2013).
15. Wang, F., Chen, C., Tan, W., Yang, K. & Yang, H. Structure of main protease from human coronavirus NL63: insights for wide spectrum anti-coronavirus drug design. *Sci. Rep*. **6**, 22677 (2016).
16. Zhao, Q. et al. Structure of the main protease from a global infectious human coronavirus, HCoV-HKU1. *J. Virol*. **82**, 8647–8655 (2008).
17. Lee, C.-C. et al. Structural basis of inhibition specificities of 3C and 3C-like proteases by zinc-coordinating and peptidomimetic compounds. *J. Biol. Chem*. **284**, 7646–7655 (2009).
18. St John, S. E., Tomar, S., Stauffer, S. R. & Mesecar, A. D. Targeting zoonotic viruses: structure-based inhibition of the 3C-like protease from bat coronavirus HKU4—the likely reservoir host to the human coronavirus that causes Middle East respiratory syndrome (MERS). *Bioorg. Med. Chem*. **23**, 6036–6048 (2015).
19. Wang, F. et al. Crystal structure of feline infectious peritonitis virus main protease in complex with synergetic dual inhibitors. *J. Virol*. **90**, 1910–1917 (2016).
20. Wang, F. et al. Michael acceptor-based peptidomimetic inhibitor of main protease from porcine epidemic diarrhea virus. *J. Med. Chem*. **60**, 3212–3216 (2017).
21. Cui, W. et al. The crystal structure of main protease from mouse hepatitis virus A59 in complex with an inhibitor. *Biochem. Biophys. Res. Commun*. **511**, 794–799 (2019).
22. Friesner, R. A. et al. Glide: a new approach for rapid, accurate docking and scoring. 1. Method and assessment of docking accuracy. *J. Med. Chem*. **47**, 1739–1749 (2004).
23. Rubin, B. & Waugh, M. H. Antiphlogistic effects of antiserotonin (SQ 10,643) and aminopyrine in rats versus endotoxin and other agents. *Proc. Soc. Exp. Biol. Med*. **119**, 438–443 (1965).
24. Chen, L. et al. Cinanserin is an inhibitor of the 3C-like proteinase of severe acute respiratory syndrome coronavirus and strongly reduces virus replication in vitro. *J. Virol*. **79**, 7095–7103 (2005).
25. Feng, B. Y. & Shoichet, B. K. A detergent-based assay for the detection of promiscuous inhibitors. *Nat. Protocols* **1**, 550–553 (2006).
26. Singh, N. et al. A safe lithium mimetic for bipolar disorder. *Nat. Commun*. **4**, 1332 (2013).
27. Lynch, E. & Kil, J. Development of ebselen, a glutathione peroxidase mimic, for the prevention and treatment of noise-induced hearing loss. *Semin. Hear*. **30**, 047–055 (2009).
28. Kil, J. et al. Safety and efficacy of ebselen for the prevention of noise-induced hearing loss: a randomised, double-blind, placebo-controlled, phase 2 trial. *Lancet* **390**, 969–979 (2017).
29. Renson, M., Etschenberg, E. & Winkelmann, J. 2-Phenyl-1, 2-benzisoselenazol-3 (2*H*)-one containing pharmaceutical preparations and process for the treatment of rheumatic diseases. US patent **4**, 352, 799 (1982).
30. Masaki, C. et al. Effects of the potential lithium-mimetic, ebselen, on impulsivity and emotional processing. *Psychopharmacology (Berl.)* **233**, 2655–2661 (2016).
31. Xu, M. et al. Identification of small-molecule inhibitors of Zika virus infection and induced neural cell death via a drug repurposing screen. *Nat. Med*. **22**, 1101–1107 (2016).
32. Aulner, N., Danckaert, A., Ihm, J., Shum, D. & Shorte, S. L. Next-generation phenotypic screening in early drug discovery for infectious diseases. *Trends Parasitol*. **35**, 559–570 (2019).

Methods

No statistical methods were used to predetermine sample size. The experiments were not randomized and investigators were not blinded to allocation during experiments and outcome assessment.

Cloning, protein expression and purification of SARS-CoV-2 M^{pro}

The full-length gene that encodes SARS-CoV-2 M^{pro} (NC_045512) was optimized and synthesized for *E. coli* expression (Genewiz). The cloning strategy for producing authentic viral M^{pro} has previously been reported[10]. The expression plasmid was transformed into *E. coli* BL21 (DE3) cells and then cultured in Luria broth medium containing 100 μg/ml ampicillin at 37 °C. When the cells were grown to an optical density at 600 nm of 0.6–0.8, 0.5 mM IPTG was added to the cell culture to induce the expression at 16 °C. After 10 h, the cells were collected by centrifugation at 3,000*g*. The cell pellets were resuspended in lysis buffer (20 mM Tris-HCl pH 8.0, 300 mM NaCl), lysed by high-pressure homogenization, and then centrifuged at 25,000*g* for 40 min. The supernatant was loaded onto Ni-NTA affinity column (Qiagen), and washed in the resuspension buffer containing 20 mM imidazole. The His-tagged M^{pro} was eluted by cleavage buffer (50 mM Tris-HCl pH 7.0, 150 mM NaCl) including 300 mM imidazole. Human rhinovirus 3C protease was added to remove the C-terminal His tag. The M^{pro} was further purified by ion-exchange chromatography and size-exclusion chromatography. Coronavirus M^{pro} exists as a mixture of monomers and dimers in solution[33]. The purified M^{pro} was stored in 50 mM Tris-HCl pH 7.3, 1 mM EDTA.

Crystallization, data collection and structure determination

SARS-CoV-2 M^{pro} was incubated with 10 mM N3 for 30 min and the complex (5 mg/ml) was crystallized by hanging drop vapour diffusion method at 20 °C. The best crystals were grown with well buffer containing 0.1 M MES pH 6.0, 2% polyethylene glycol (PEG) 6000, 3% DMSO, 1 mM DTT. The cryo-protectant solution contained 0.1 M MES pH 6.0, 30% PEG 400.

X-ray data were collected on beamline BL17U1 at Shanghai Synchrotron Radiation Facility (SSRF) at 100 K and at a wavelength of 1.07180 Å using an Eiger X 16M image plate detector. Data integration and scaling were performed using the program Xia2[34]. The structure was determined by molecular replacement with the Phaser module[35] in CCP4[36] using the SARS-CoV M^{pro} (RCSP Protein Data Bank code (PDB) 2H2Z) as a search template. The output model from molecular replacement was subsequently subjected to iterative cycles of manual model adjustment with Coot[37] and refinement was finished with Phenix[38]. The inhibitor N3 was built according to the omit map. The phasing and refinement statistics are summarized in Extended Data Table 1. The R_{work} and R_{free} values are 0.202 and 0.235, respectively. There are 97.3% of the residues in the most favoured regions of the Ramachandran plot, and no residues are found in disallowed regions.

Enzymatic activity and inhibition assays

The enzyme activity assays have previously been described[10]. In brief, the activity of SARS-CoV-2 M^{pro} was measured by a continuous kinetic assay, with the substrate Mca–AVLQ↓SGFR-K(Dnp)K (GL Biochem), using wavelengths of 320 nm and 405 nm for excitation and emission, respectively. The assay started by immediately mixing 0.2 μM SARS-CoV-2 M^{pro} with different concentrations of substrate (2.5–100 μM). Fluorescence intensity was monitored with an EnVision multimode plate reader (Perkin Elmer). Initial rates were obtained by fitting the linear portion of the curves to a straight line. The kinetic parameters K_m and k_{cat} were calculated from a double-reciprocal plot. As N3 is a mechanism-based irreversible inhibitor for SARS-CoV-2 M^{pro}, $k_{obs}/[I]$ was used as an approximation of the pseudo-second-order rate constant to evaluate the inhibition effect of the inhibitor N3 (ref. [12]). In this case, the measurement was carried out with 0.2 μM of enzyme, 20 μM of substrate and inhibitor at 6 different concentrations (0–1 μM).

Virtual screening

The virtual screening was performed using our in-house database via a workflow application of Glide (v.8.2)[22] in Maestro (Schrödinger 2019-1a). All compounds in the database were considered to be at pH 7.4 ± 0.2 to estimate their protonation state using the program EpiK[39]. Their three-dimensional (3D) conformations were generated by the ligPrep module of Maestro. The structure of SARS-CoV-2 M^{pro} (PDB 6LU7) was used to generate the receptor grid for docking simulations. The centre of the active site of the grid was determined according to the position of N3 in the structure. The flexibility of the receptor hydroxyl and thiol groups in side chains of C145, S46 and Y54 were considered. At the very beginning, we performed a relatively fast but raw screening using the Glide standard precision model, and the top 20% of compounds were kept. Finally, the candidate molecules were picked by analysing the predicted binding modes and their scores.

High-throughput drug screening and IC_{50} measurement

Potential inhibitors against SARS-CoV-2 M^{pro} were screened by an enzymatic inhibition assay. When the different compounds were added into the enzymatic reaction mixture, the change of initial rates was calculated to evaluate their inhibitory effect. Five drug libraries—the Approved Drug Library (Target Mol), Clinic Compound Library (Target Mol), FDA-approved Drug Library (Selleck), Natural Product Library (Selleck), and Anti-virus Drug Library (Shanghai Institute for Advanced Immunochemical Studies)—that together comprised about 10,000 compounds were used. The preliminary screening reaction mixture included 0.2 μM protein, 20 μM substrate and 50 μM compounds. The compounds of interest were defined as those with a percentage of inhibition over 60% compared with the reaction in the absence of inhibitor. IC_{50} values of 7 drug leads were measured using 0.2 μM protein, 20 μM substrate and 11 different inhibitor concentrations. To exclude inhibitors possibly acting as aggregators, a detergent-based control was performed by adding 0.001% or 0.01% freshly made up Triton X-100 to the reaction at the same time[25]. All experimental data was analysed using GraphPad Prism. All experiments were performed in triplicate.

Molecular docking

To understand the binding interaction of these molecules with SARS-CoV-2 M^{pro}, two different molecular docking methods (Glide (v.8.2)[22] and iFitDock[40]) were used to predict their binding poses. Then, a 3D molecular similarity calculation method, SHAFTS[41], was used for enumeration of the molecular alignment poses by matching the critical pharmacophore and volumetric overlay between the N3 molecule within the M^{pro} structure and the other drug candidates. Then, the obtained optimal superposition of these molecules was used to assess the reasonability of the predicted binding poses from the two docking methods, and only the binding orientations that were consistent among different methods were kept for constructing the initial complexes. Finally, these complexes were further optimized and re-scored using the MM-GBSA module[42] of Schrödinger, and the residues within 5 Å around the ligand were refined.

Antiviral and cytotoxicity assays for compounds from high-throughput screening

The in vitro antiviral efficacy of the drug candidates on Vero cells was determined by qRT–PCR. About 1×10^4 Vero cells were seeded into a 96-well plate and incubated for 20–24 h at 37 °C. All the infection experiments were performed at biosafety level-3 (BSL-3). Cells were pretreated with the drug candidates (10 μM) for 1 h; SARS-CoV-2 (multiplicity of infection (MOI) of 0.01) was subsequently added to allow infection for 2 h. Then, the virus–drug mixture was removed and cells were further cultured with fresh drug-containing medium. At 72 h after infection, vRNA was extracted from the culture supernatant

using QIAamp viral RNA mini kit (Qiagen) according to the manufacturer's recommendation, and detected by qRT–PCR assay using the SARS-CoV-2-specific primers. Because shikonin showed cellular toxicity at the test concentration, its antiviral activity assay did not proceed further. vRNA copies per millilitre were determined using a synthetic RNA fragment to amplify the target region. The linearized plasmid containing the *S* gene of SARS-CoV-2 was subjected to in vitro transcription. The resulting RNA transcripts were purified and then quantified using spectrophotometry on Nanodrop 2000 (Thermo Fisher Scientific). The purified RNA was diluted tenfold serially using RNase-free water and was detected using qRT–PCR. Threshold cycle (C_t) values for the known concentrations of the RNA were plotted against the log of the number of genome-equivalent copies. The resultant standard curve was used to determine the number of genome equivalents of vRNA in the samples. The determination of the detection limit was based on the lowest level at which vRNA was detected and remained within the range of linearity of a standard curve (C_t value of 38). TaqMan primers for SARS-CoV-2 are 5′-TCCTGGTGATTCTTCTTCAGG-3′ and 5′-TCTGAGAGAGGGTCAAGTGC-3′ with SARS-CoV-2 probe 5′-FAM-AGCTGCAGCACCAGCTGTCCA-BHQ1-3′. The cytotoxicity of the tested drugs on Vero cell were determined by MTS cell proliferation assays (Promega). Ten thousand cells were seeded into a 96-well plate and incubated for 20–24 h at 37 °C. After that, the medium was removed, and 100 µl of medium containing decreasing concentrations of antiviral compounds was added to the wells. After 4 days incubation at 37 °C, MTS assays were performed according to manufacturer's protocols. All experiments were performed in triplicate. Vero cells were obtained from ATCC (American Type Culture Collection) with authentication service. All cell lines tested negative for mycoplasma contamination. No commonly misidentified cell lines were used.

Antiviral and cytotoxicity assays for cinanserin

For the antiviral assay, a clinical isolate of SARS-CoV-2[3] was propagated in Vero E6 cells, and viral titre was determined as previously described[43]. All of the infection experiments were performed at BSL-3. Preseeded Vero E6 cells (5×10^4 cells per well) were pretreated with the different concentrations of cinanserin for 1 h and the virus was subsequently added (MOI of 0.05) to allow infection for 2 h. Then, the virus–drug mixture was removed and cells were further cultured with fresh drug-containing medium. At 24 h after infection, the cell supernatant was collected and vRNA in supernatant was subjected to qRT–PCR analysis. For cytotoxicity assays, Vero E6 cells were suspended in growth medium in 96-well plates. The next day, appropriate concentrations of cinanserin were added to the medium. After 24 h, the relative numbers of surviving cells were measured by CCK8 (Beyotime) assay in accordance with the manufacturer's instructions. All experiments were performed in triplicate. Vero E6 cells were obtained from ATCC with authentication service. All cell lines tested negative for mycoplasma contamination. No commonly misidentified cell lines were used.

Plaque-reduction assays

One hundred thousand Vero E6 cells were seeded in a 24-well plate and treated with different doses of the inhibitors. All of the infection experiments were performed at BSL-3. Inhibitors with different dilution concentrations were mixed with SARS-CoV-2 (100 plaque-forming units), and 200 µl mixtures were inoculated onto monolayer Vero E6 cells for 1 h. After removing the supernatant, the plate was washed twice with DMEM medium, cells were incubated with 0.9% agarose containing appropriate concentrations of inhibitors. The overlay was discarded at 4 days after infection, and cells were fixed for 30 min in 4% polyoxymethylene and stained with crystal violet working solution. The plaque-forming units were determined. All experiments were performed in four biological replicates.

Intact protein analysis

In brief, 2.5 µl of compounds (10 mM in DMSO) was added into 50 µl of SARS-CoV-2 M^{pro} (10 mg/ml). The mixtures were kept at room temperature for 30 min. Liquid chromatography–mass spectrometry analyses were performed in positive-ion mode with a quadrupole-time-of-flight mass spectrometer (Agilent 6550) coupled with a high-performance liquid chromatograph (HPLC, Agilent 1260) for detecting the molecular weight of intact proteins. The samples were eluted from a Phenomenex Jupiter C4 300Å LC column (2 × 150 mm, 5 µm) over a 15-min gradient from 5% to 100% acetonitrile containing 0.1% formic acid at a flow rate of 0.5 ml/min. The acquisition method in positive-ion mode with Dual Agilent Jet Stream electrospray voltage used a capillary temperature of 250 °C, a fragmentor of 175 V and a capillary voltage of 3,000 V. Mass deconvolution was performed using Agilent MassHunter Qualitative Analysis B.06.00 software with BioConfirm Workflow.

Tandem mass spectrometry analysis

The samples were precipitated and redissolved by 8 M urea, and then digested for 16 h at 25 °C by chymotrypsin at an enzyme-to-substrate ratio of 1:50 (w/w). The digested peptides were desalted and loaded onto a homemade 30-cm-long pulled-tip analytical column (ReproSil-Pur C18 AQ 1.9-µm particle size, Dr Maisch, 75-µm inner diameter × 360-µm outer diameter) connected to an Easy-nLC1200 UHPLC (Thermo Fisher Scientific) for mass spectrometry analysis. The elution gradient and mobile phase constitution used for peptide separation were as follows: 0–1 min, 4–8% B; 1–96 min, 8–35% B; 96–104 min, 35–60% B; 105–120 min, 60–100% B (mobile phase A: 0.1% formic acid in water; mobile phase B: 0.1% formic acid in 80% acetonitrile) at a flow rate of 300 nl/min. Peptides eluted from the liquid chromatography column were directly electro-sprayed into the mass spectrometer with the application of a distal 1.8-kV spray voltage. Survey full-scan mass spectra (from m/z 300–1,800) were acquired in the Orbitrap analyser (Q Exactive, Thermo Fisher Scientific) with resolution r = 70,000 at m/z 400. The top 20 tandem mass spectrometry (MS/MS) events were sequentially generated and selected from the full mass spectrum at a 30% normalized collision energy. The dynamic exclusion time was set to 10 s. One acquisition cycle includes one full-scan mas spectrum followed by top 20 MS/MS events, sequentially generated on the first to the twentieth most intense ions selected from the full mass spectrum at a 28% normalized collision energy. The acquired MS/MS data were analysed using the UniProtKB *E. coli* database (database released on 11 November 2016) and SARS-CoV-2 nsp5, using Protein Discoverer 2.1. To accurately estimate peptide probabilities and false-discovery rates, we used a decoy database containing the reversed sequences of all the proteins appended to the target database. The false-discovery rate was set to 0.01. Mass tolerance for precursor ions was set to 20 ppm. Chymotrypsin was defined as cleavage enzyme and the maximal number of missed cleavage sites was set to four. Protein N terminus acetylation, methionine oxidation and compounds covalent bindings were set as variable modifications. The modified peptides were manually checked and labelled.

Reporting summary

Further information on research design is available in the Nature Research Reporting Summary linked to this paper.

Data availability

The coordinates and structure factors for SARS-CoV-2 M^{pro} in complex with the inhibitor N3 have been deposited in the PDB with accession number 6LU7, deposited on the 26 January 2020 and released on the 5 February 2020. While this work was under review, we solved the complex structure at a higher resolution (1.7 Å); the relevant coordinates and structure factors have been deposited in the PDB with accession

number 7BQY. Any other relevant data are available from the corresponding authors upon reasonable request.

33. Anand, K., Ziebuhr, J., Wadhwani, P., Mesters, J. R. & Hilgenfeld, R. Coronavirus main proteinase ($3CL^{pro}$) structure: basis for design of anti-SARS drugs. *Science* **300**, 1763–1767 (2003).
34. Winter, G. xia2: an expert system for macromolecular crystallography data reduction. *J. Appl. Crystallogr.* **43**, 186–190 (2010).
35. McCoy, A. J. et al. Phaser crystallographic software. *J. Appl. Crystallogr.* **40**, 658–674 (2007).
36. Potterton, L. et al. CCP4i2: the new graphical user interface to the CCP4 program suite. *Acta Crystallogr. D* **74**, 68–84 (2018).
37. Emsley, P., Lohkamp, B., Scott, W. G. & Cowtan, K. Features and development of Coot. *Acta Crystallogr. D* **66**, 486–501 (2010).
38. Afonine, P. V. et al. Towards automated crystallographic structure refinement with phenix. refine. *Acta Crystallogr. D* **68**, 352–367 (2012).
39. Greenwood, J. R., Calkins, D., Sullivan, A. P. & Shelley, J. C. Towards the comprehensive, rapid, and accurate prediction of the favorable tautomeric states of drug-like molecules in aqueous solution. *J. Comput. Aided Mol. Des.* **24**, 591–604 (2010).
40. Bai, F. et al. Free energy landscape for the binding process of huperzine A to acetylcholinesterase. *Proc. Natl Acad. Sci. USA* **110**, 4273–4278 (2013).
41. Liu, X., Jiang, H. & Li, H. SHAFTS: a hybrid approach for 3D molecular similarity calculation. 1. Method and assessment of virtual screening. *J. Chem. Inf. Model.* **51**, 2372–2385 (2011).
42. Guimarães, C. R. W. & Cardozo, M. MM-GB/SA rescoring of docking poses in structure-based lead optimization. *J. Chem. Inf. Model.* **48**, 958–970 (2008).
43. Wang, M. et al. Remdesivir and chloroquine effectively inhibit the recently emerged novel coronavirus (2019-nCoV) in vitro. *Cell Res.* **30**, 269–271 (2020).

Acknowledgements We thank Y. Lei and J. Kong from High Throughput Platform and staff from Analytical Chemistry Platform at the Shanghai Institute for Advanced Immunochemical Studies for their technical support; the National Centre for Protein Science Shanghai and The Molecular and Cell Biology Core Facility of the School of Life Science and Technology, ShanghaiTech University for use of their instrumentation and technical assistance; Z. Liu and H. Su for discussion; and the staff from beamlines BL17U1, BL18U1 and BL19U1 at the Shanghai Synchrotron Radiation Facility. This work was supported by grants from National Key R&D Program of China (grant no. 2017YFC0840300 to Z.R. and no. 2020YFA0707500), Project of International Cooperation and Exchanges NSFC (grant no. 81520108019 to Z.R.), Science and Technology Commission of Shanghai Municipality (grant no. 20431900200) and Department of Science and Technology of Guangxi Zhuang Autonomous Region (grant no. 2020AB40007).

Author contributions Z.R. and H.Y. conceived the project; Z.J., H.J., Z.R. and H.Y. designed the experiments; Z.J., X.D., Y. Duan, J.Y., T.Y., Xiaoce Liu and Xiuna Yang cloned, expressed, purified and crystallized proteins; Z.J., Y.Z., B.Z. and F.L. collected the diffraction data; B.Z. and Xiang Liu solved the crystal structure; Z.J., X.D., Y. Duan and J.Y. performed enzymatic activity and inhibition assays, high-throughput drug screening and IC_{50} measurements; L.W. and F.B. performed virtual screening and molecular docking; Y.X., L.Z. and H.L. performed enzymatic inhibition, cell-based antiviral and cytotoxicity assays for cinanserin; Y. Deng and X.L. performed qRT–PCR analysis and cytotoxicity assay of N3; M.L., R.J. and Xinglou Yang performed plaque-reduction assays; C.P. performed intact protein and MS/MS analyses; Z.J., X.D., Y.X., Y. Deng, C.P., F.B., H.L., Xiang Liu, K.Y., L.G., W.X., G.X., C.Q., Z.S., H.J., Z.R. and H.Y. analysed and discussed the data; Z.J., X.D., F.B., Xiang Liu, L.G., G.X., C.Q., Z.S., H.J., Z.R. and H.Y. wrote the manuscript.

Competing interests The authors declare no competing interests.

Additional information

Supplementary information is available for this paper at https://doi.org/10.1038/s41586-020-2223-y.

Correspondence and requests for materials should be addressed to H.J., Z.R. or H.Y.

Peer review information *Nature* thanks Julien Lescar and the other, anonymous, reviewer(s) for their contribution to the peer review of this work.

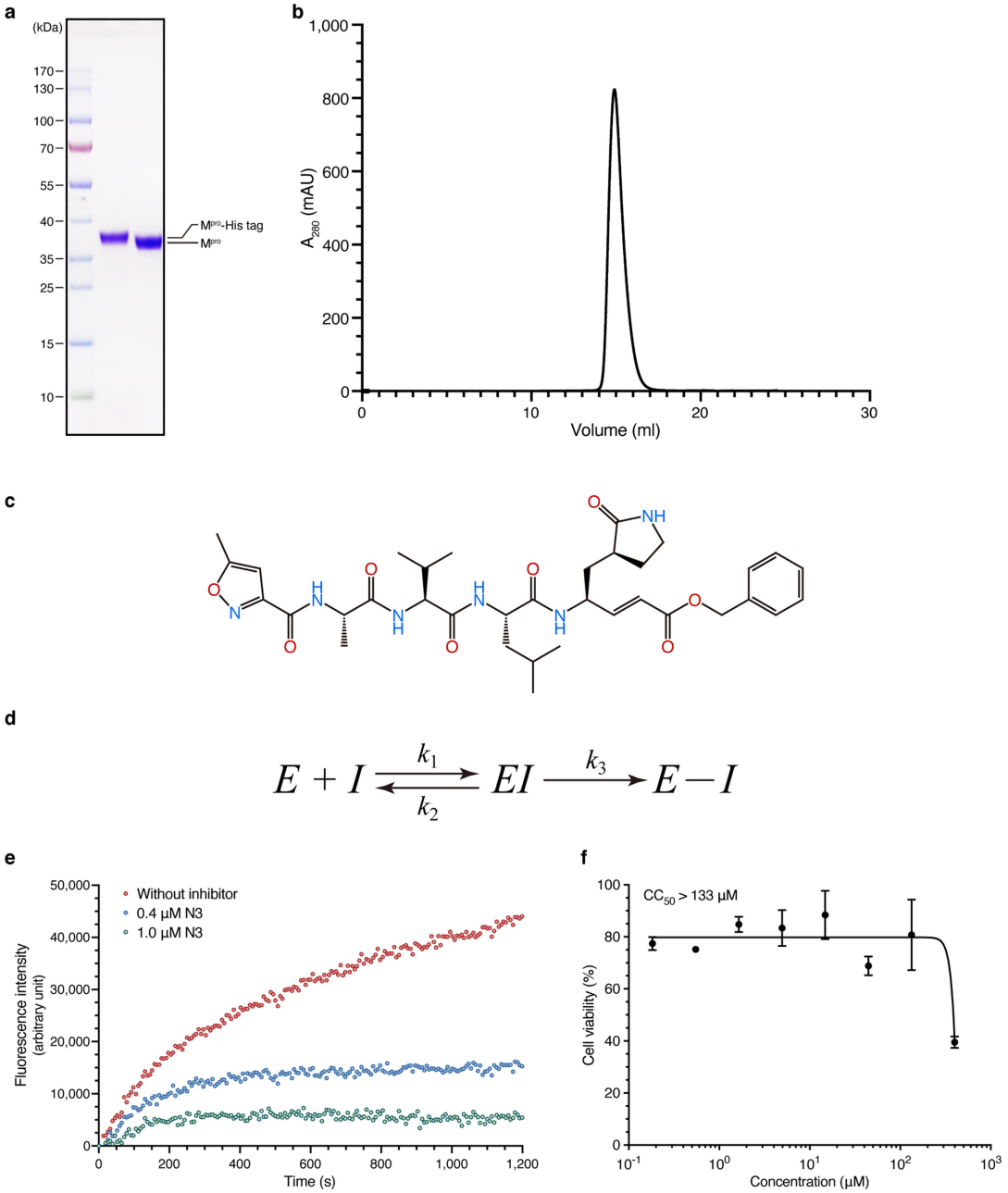

Extended Data Fig. 1 | The purification of SARS-CoV-2 M^{pro} and the inhibitory assay of the N3 compound. a, SDS–PAGE gel of SARS-CoV-2 M^{pro}. First lane, marker; second lane, M^{pro} before treating with rhinovirus 3C protease; third lane, M^{pro} after the cleavage of C-terminal His tag. For gel source data, see Supplementary Fig. 1. **b**, Size-exclusion chromatography profile of M^{pro}. **c**, The chemical structure of the N3 inhibitor. **d**, Inhibition mechanism for N3. **e**, Typical inhibition curves for N3. **f**, Cytotoxicity assay of N3 on Vero cells. Data are shown as mean ± s.e.m., $n = 3$ biological replicates. The data in **a**, **b**, **e**, **f** are representative of three independent experiments with similar results.

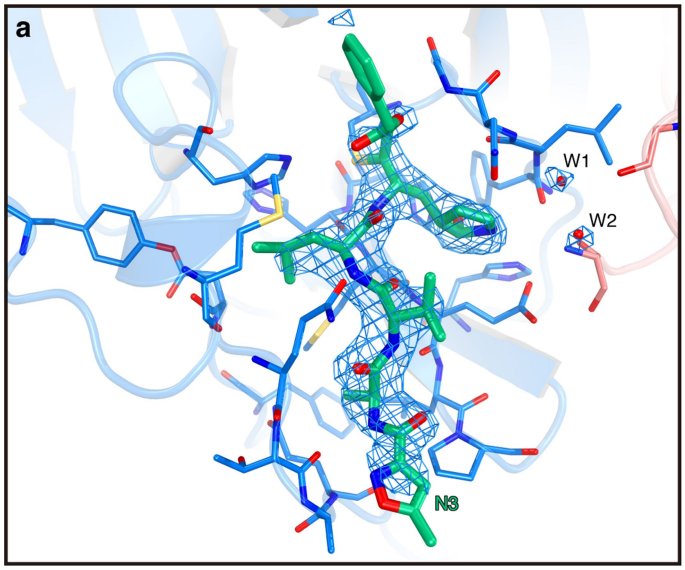

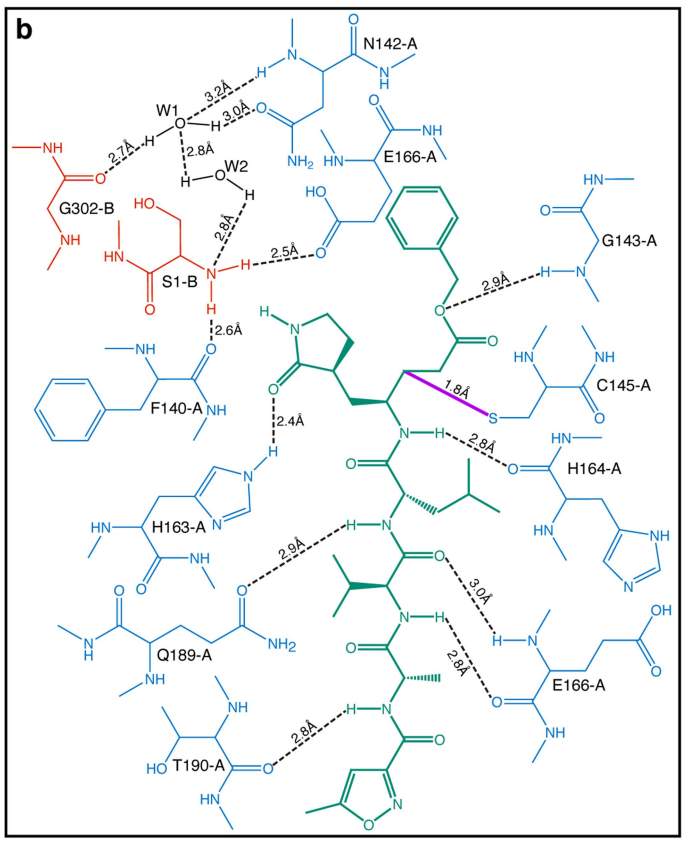

Extended Data Fig. 2 | The interactions between SARS-CoV-2 M^{pro} and N3. **a**, The $F_o - F_c$ omit map (contour level of 3σ, shown as blue mesh). **b**, Detailed view of the interactions between the inhibitor N3 and SARS-CoV-2 M^{pro}. M^{pro} residues are shown in blue (protomer A) and salmon (protomer B); N3 is in green; and water is in black. The hydrogen bonds are shown as black dashed lines. The covalent bond between N3 and the C145 of protomer A is in purple.

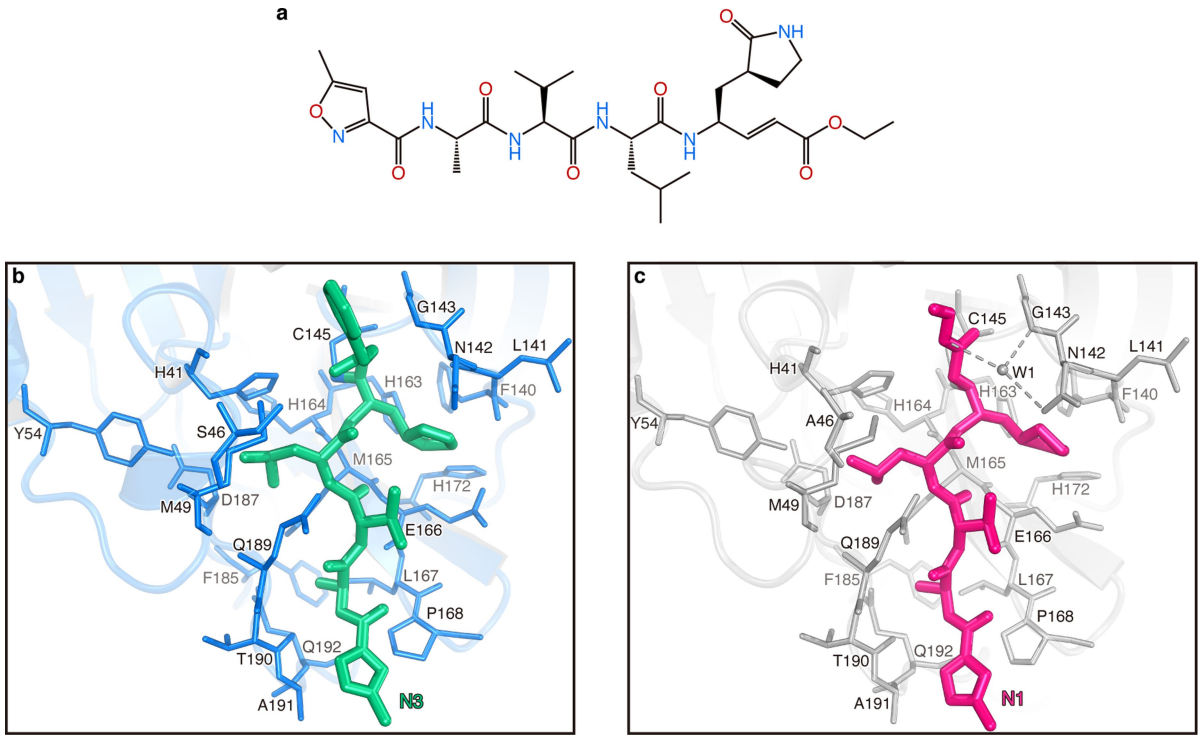

Extended Data Fig. 3 | Comparison of the binding modes between SARS-CoV-2 M^{pro}–N3 and SARS-CoV M^{pro}–N1. a, The chemical structure of the N1 inhibitor. **b**, The binding mode of SARS-CoV-2 M^{pro} (blue sticks) with N3 (green sticks). **c**, The binding mode of SARS-CoV M^{pro} (grey sticks) with N1 (pink sticks). The hydrogen bonds formed by water (W1) are indicated by the dashed lines.

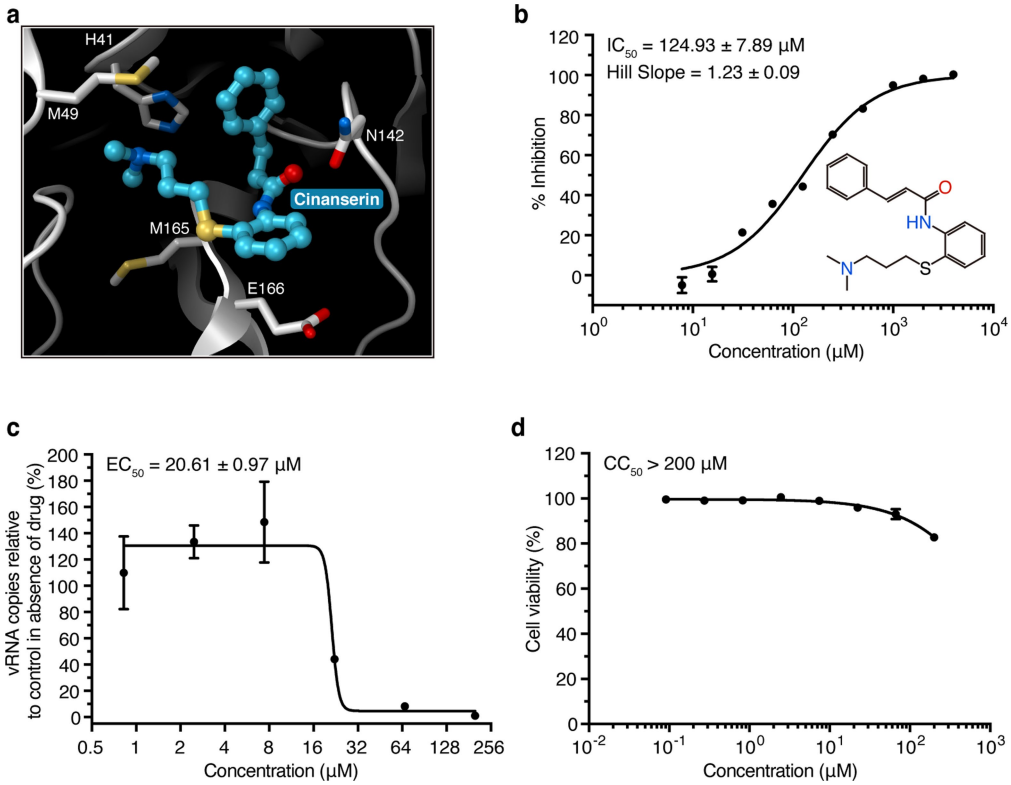

Extended Data Fig. 4 | Cinanserin is an inhibitor of SARS-CoV-2 M^{pro}. a, The docking result of cinanserin. The structure of SARS-CoV-2 M^{pro} is shown as a white cartoon, cinanserin is shown as cyan balls and sticks, and residues predicted to be interacting with cinanserin are shown as sticks. **b**, Inhibitory activity of cinanserin on M^{pro}. **c**, Antiviral activity of cinanserin determined by qRT–PCR. **d**, Cytotoxicity assay of cinanserin on Vero E6 cells. All data are shown as mean ± s.e.m., $n = 3$ biological replicates.

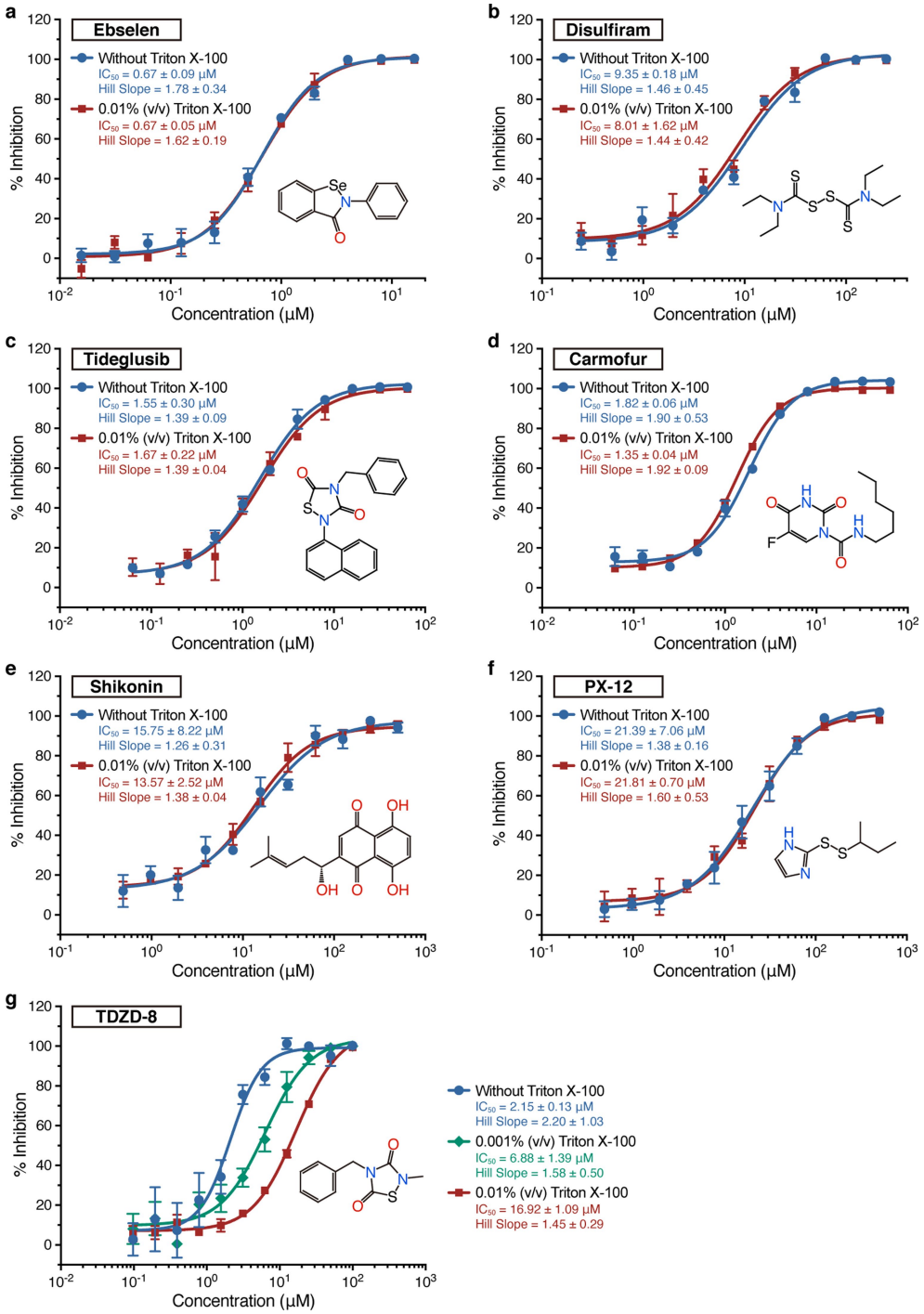

Extended Data Fig. 5 | The detergent-based assay for drug leads. a–f, The IC_{50} values determined in the presence or absence of 0.01% Triton X-100, which show that detergent did not affect the results. **g**, Different concentrations of Triton X-100 notably affected IC_{50} curves for TDZD-8. All data are shown as mean ± s.e.m., $n = 3$ biological replicates.

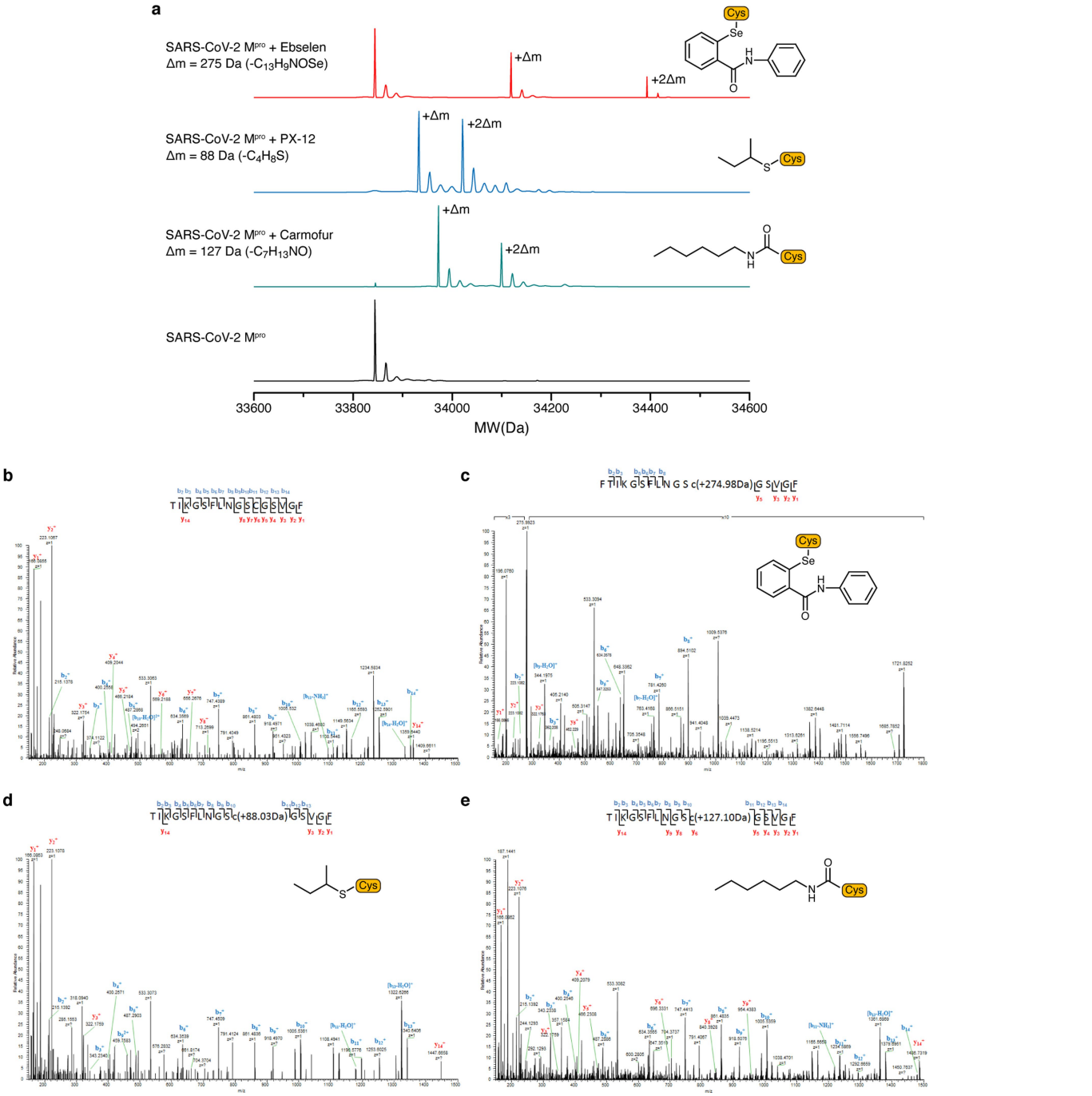

Extended Data Fig. 6 | MS/MS analysis reveals that ebselen, PX-12 and carmofur are able to covalently bind to C145 of SARS-CoV-2 M^{pro}. **a**, Molecular weight of apo SARS-CoV-2 M^{pro} and compound-treated M^{pro}. The mass shifts (Δm) of the proteins indicate that more than one molecular of the compounds can be covalently bonded to one molecular of M^{pro}. **b**–**e**, A higher-energy collisional dissociation MS/MS spectrum recorded on the $[M+H]^{2+}$ ion, at *m/z* 787.3852 of the M^{pro} unmodified peptide TIKGSFLNGSCGSVGF (**b**); at *m/z* 998.4152 of the M^{pro} modified peptide FTIKGSFLNGSCGSVGF containing a modification ($-C_{13}H_9NOSe$) induced by ebselen on C145 (**c**); at *m/z* 831.4080 of the M^{pro} modified peptide TIKGSFLNGSCGSVGF containing a modification($-C_4H_8S$) induced by PX-12 on C145 (**d**); and at *m/z* 850.9414 of the M^{pro} modified peptide TIKGSFLNGSCGSVGF containing a modification($-C_7H_{13}NO$) induced by carmofur on C145 (**e**). Some of the predicted b- and y-type ions are listed above and below the peptide sequence, respectively. The experiment was performed once.

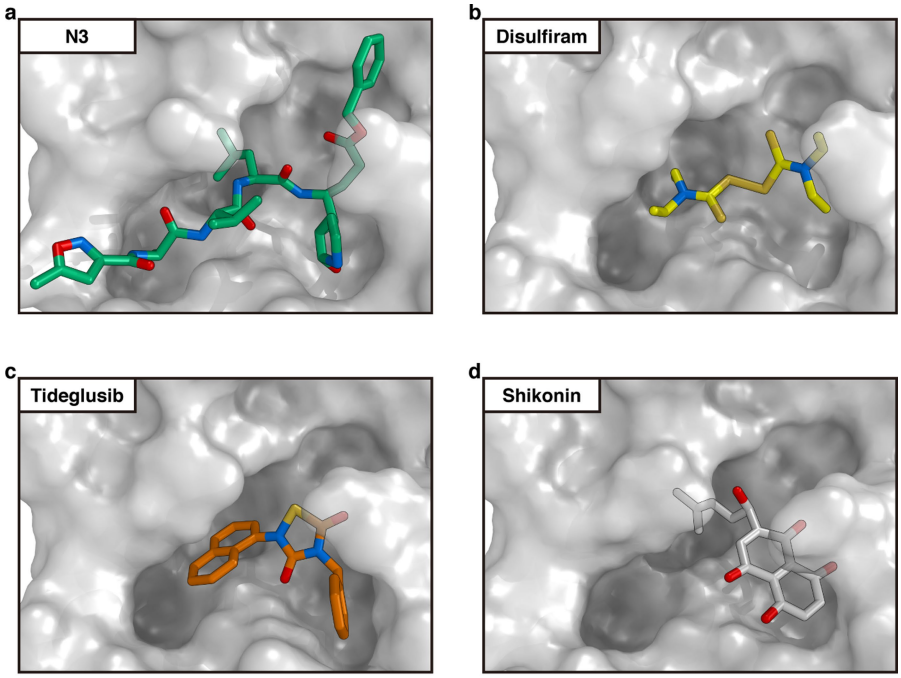

e

Drug	Predicted ΔG_{bind} (kcal/mol)
Disulfiram	-46.16
Tideglusib	-61.79
Shikonin	-47.35

Extended Data Fig. 7 | Docking poses of different SARS-CoV-2 M^{pro} inhibitors. a, The crystal structure of the SARS-CoV-2 M^{pro}–N3 complex. **b**–**d**, The docking results of three drug leads. M^{pro} is shown as grey background, and inhibitors are shown in different colours. The inhibitors identified through the high-throughput screening are likely to occupy the same pocket as N3. **e**, Predicted binding affinities for the drug leads to SARS-CoV-2 M^{pro} by using the MM-GBSA module, integrated in Schrödinger.

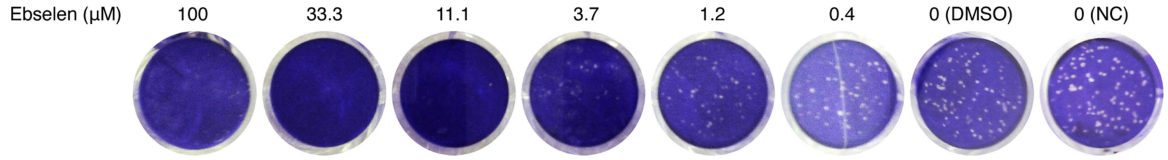

Extended Data Fig. 8 | Images for the plaque-reduction assay using ebselen. As the concentration of ebselen increases, there is a considerable reduction in the numbers of the plaques in comparison to the negative control (NC) and DMSO. Results are shown as representative of four biological replicates. For image source data, see Supplementary Fig. 2.

Extended Data Table 1 | Data collection and refinement statistics

	PDB code: 6LU7*
Data collection	
Space group	*C*2
Cell dimensions	
a, *b*, *c* (Å)	97.931, 79.477, 51.803
α, β, γ (°)	90, 114.55, 90
Resolution (Å)	50.00-2.16 (2.22-2.16)†
R_{merge}	18.9 (147.2)
$I / \sigma I$	6.3 (3.2)
Completeness (%)	100.0 (100.0)
Redundancy	6.6 (6.1)
Refinement	
Resolution (Å)	50.00-2.16
No. reflections	19455 (1431)
R_{work} / R_{free}	0.2020/0.2350
No. atoms	
Protein	2367
Ligand/ion	49
Water	84
B-factors	
Protein	42.7
Ligand/ion	46.3
Water	44.2
R.m.s. deviations	
Bond lengths (Å)	0.002
Bond angles (°)	0.474

*A single crystal was used for data collection and structure determination.

†Values in parentheses are for the highest-resolution shell.

nature research

Corresponding author(s): Hualiang Jiang, Zihe Rao & Haitao Yang

Last updated by author(s): Mar 28, 2020

Reporting Summary

Nature Research wishes to improve the reproducibility of the work that we publish. This form provides structure for consistency and transparency in reporting. For further information on Nature Research policies, see Authors & Referees and the Editorial Policy Checklist.

Statistics

For all statistical analyses, confirm that the following items are present in the figure legend, table legend, main text, or Methods section.

n/a	Confirmed	
☐	☒	The exact sample size (*n*) for each experimental group/condition, given as a discrete number and unit of measurement
☐	☒	A statement on whether measurements were taken from distinct samples or whether the same sample was measured repeatedly
☒	☐	The statistical test(s) used AND whether they are one- or two-sided *Only common tests should be described solely by name; describe more complex techniques in the Methods section.*
☒	☐	A description of all covariates tested
☒	☐	A description of any assumptions or corrections, such as tests of normality and adjustment for multiple comparisons
☐	☒	A full description of the statistical parameters including central tendency (e.g. means) or other basic estimates (e.g. regression coefficient) AND variation (e.g. standard deviation) or associated estimates of uncertainty (e.g. confidence intervals)
☒	☐	For null hypothesis testing, the test statistic (e.g. *F*, *t*, *r*) with confidence intervals, effect sizes, degrees of freedom and *P* value noted *Give P values as exact values whenever suitable.*
☒	☐	For Bayesian analysis, information on the choice of priors and Markov chain Monte Carlo settings
☒	☐	For hierarchical and complex designs, identification of the appropriate level for tests and full reporting of outcomes
☒	☐	Estimates of effect sizes (e.g. Cohen's *d*, Pearson's *r*), indicating how they were calculated

Our web collection on statistics for biologists contains articles on many of the points above.

Software and code

Policy information about availability of computer code

Data collection	Blu-Ice BL17U1; EnVision Manager (v1.13.3009.1409)
Data analysis	Xia2 (v0.3.8.0); HKL2000 (v712); CCP4 (v7.0.077); Coot (v0.8.9.2); Phenix (v1.17.1-3660); Glide (v8.2); Maestro (Schrödinger 2019-1); EpiK (Schrödinger 2019-1); GraphPad Prism (v8.3.1); Microsoft Excel (v16.35); PyMOL (v2.3.4); iFitDock (1.0); SHAFTS (1.0); MM-GBSA (Schrödinger 2019-1); Agilent MassHunter Qualitative Analysis (B.06.00); Protein Discoverer (2.1)

For manuscripts utilizing custom algorithms or software that are central to the research but not yet described in published literature, software must be made available to editors/reviewers. We strongly encourage code deposition in a community repository (e.g. GitHub). See the Nature Research guidelines for submitting code & software for further information.

Data

Policy information about availability of data

All manuscripts must include a data availability statement. This statement should provide the following information, where applicable:

- Accession codes, unique identifiers, or web links for publicly available datasets
- A list of figures that have associated raw data
- A description of any restrictions on data availability

The PDB accession No. for the coordinates of COVID-19 virus main protease in complex with N3 is 6LU7.

Field-specific reporting

Please select the one below that is the best fit for your research. If you are not sure, read the appropriate sections before making your selection.

☒ Life sciences ☐ Behavioural & social sciences ☐ Ecological, evolutionary & environmental sciences

For a reference copy of the document with all sections, see nature.com/documents/nr-reporting-summary-flat.pdf

Life sciences study design

All studies must disclose on these points even when the disclosure is negative.

Sample size	Sample size estimation was not relevant for this study, as it does not report on a statistical evaluation of effects between two or more groups.
Data exclusions	Samples deemed to be technical failures were excluded. Two data points were verified to be extreme outliers and were therefore removed when calculating the IC50 values: Extended Data Fig. 5a (0.0625 µM ebselen with 0.01% Triton X-100, one of the three biological replicates) Extended Data Fig. 5g (0.390625 µM TDZD-8 with 0.001% Triton X-100, one of the three biological replicates) Removal of these data points do not alter any conclusions made in this study.
Replication	To ensure reproducibility of experimental findings, each assay was performed at least three times to confirm the results. IC50 measurements (Fig. 3; Extended Data Fig. 4b; Extended Data Fig. 5) were carried out with three biological replicates for each data point and these data were used to calculate mean values. Antiviral activity assays (qRT-PCR, shown in Fig. 4a and Extended Data Fig. 4c) were performed in three biological replicates. Antiviral activity assays (plaque-reduction assays, shown in Fig. 4b, c and Extended Data Fig. 8) were carried out with four biological replicates. Cytotoxicity assays (Extended Data Fig. 1f; Extended Data Fig. 4d) were carried out with three biological replicates.
Randomization	Animals or human research participants were not involved in this study and, as such, samples were not randomized for the experiments.
Blinding	Animals or human research participants were not involved in this study and, as such, samples were not blinded for the experiments.

Behavioural & social sciences study design

All studies must disclose on these points even when the disclosure is negative.

Study description	*Briefly describe the study type including whether data are quantitative, qualitative, or mixed-methods (e.g. qualitative cross-sectional, quantitative experimental, mixed-methods case study).*
Research sample	*State the research sample (e.g. Harvard university undergraduates, villagers in rural India) and provide relevant demographic information (e.g. age, sex) and indicate whether the sample is representative. Provide a rationale for the study sample chosen. For studies involving existing datasets, please describe the dataset and source.*
Sampling strategy	*Describe the sampling procedure (e.g. random, snowball, stratified, convenience). Describe the statistical methods that were used to predetermine sample size OR if no sample-size calculation was performed, describe how sample sizes were chosen and provide a rationale for why these sample sizes are sufficient. For qualitative data, please indicate whether data saturation was considered, and what criteria were used to decide that no further sampling was needed.*
Data collection	*Provide details about the data collection procedure, including the instruments or devices used to record the data (e.g. pen and paper, computer, eye tracker, video or audio equipment) whether anyone was present besides the participant(s) and the researcher, and whether the researcher was blind to experimental condition and/or the study hypothesis during data collection.*
Timing	*Indicate the start and stop dates of data collection. If there is a gap between collection periods, state the dates for each sample cohort.*
Data exclusions	*If no data were excluded from the analyses, state so OR if data were excluded, provide the exact number of exclusions and the rationale behind them, indicating whether exclusion criteria were pre-established.*
Non-participation	*State how many participants dropped out/declined participation and the reason(s) given OR provide response rate OR state that no participants dropped out/declined participation.*
Randomization	*If participants were not allocated into experimental groups, state so OR describe how participants were allocated to groups, and if allocation was not random, describe how covariates were controlled.*

Ecological, evolutionary & environmental sciences study design

All studies must disclose on these points even when the disclosure is negative.

Study description	*Briefly describe the study. For quantitative data include treatment factors and interactions, design structure (e.g. factorial, nested, hierarchical), nature and number of experimental units and replicates.*
Research sample	*Describe the research sample (e.g. a group of tagged Passer domesticus, all Stenocereus thurberi within Organ Pipe Cactus National Monument), and provide a rationale for the sample choice. When relevant, describe the organism taxa, source, sex, age range and any manipulations. State what population the sample is meant to represent when applicable. For studies involving existing datasets, describe the data and its source.*
Sampling strategy	*Note the sampling procedure. Describe the statistical methods that were used to predetermine sample size OR if no sample-size calculation was performed, describe how sample sizes were chosen and provide a rationale for why these sample sizes are sufficient.*
Data collection	*Describe the data collection procedure, including who recorded the data and how.*
Timing and spatial scale	*Indicate the start and stop dates of data collection, noting the frequency and periodicity of sampling and providing a rationale for these choices. If there is a gap between collection periods, state the dates for each sample cohort. Specify the spatial scale from which the data are taken*
Data exclusions	*If no data were excluded from the analyses, state so OR if data were excluded, describe the exclusions and the rationale behind them, indicating whether exclusion criteria were pre-established.*
Reproducibility	*Describe the measures taken to verify the reproducibility of experimental findings. For each experiment, note whether any attempts to repeat the experiment failed OR state that all attempts to repeat the experiment were successful.*
Randomization	*Describe how samples/organisms/participants were allocated into groups. If allocation was not random, describe how covariates were controlled. If this is not relevant to your study, explain why.*
Blinding	*Describe the extent of blinding used during data acquisition and analysis. If blinding was not possible, describe why OR explain why blinding was not relevant to your study.*

Did the study involve field work? ☐ Yes ☐ No

Field work, collection and transport

Field conditions	*Describe the study conditions for field work, providing relevant parameters (e.g. temperature, rainfall).*
Location	*State the location of the sampling or experiment, providing relevant parameters (e.g. latitude and longitude, elevation, water depth).*
Access and import/export	*Describe the efforts you have made to access habitats and to collect and import/export your samples in a responsible manner and in compliance with local, national and international laws, noting any permits that were obtained (give the name of the issuing authority, the date of issue, and any identifying information).*
Disturbance	*Describe any disturbance caused by the study and how it was minimized.*

Reporting for specific materials, systems and methods

We require information from authors about some types of materials, experimental systems and methods used in many studies. Here, indicate whether each material, system or method listed is relevant to your study. If you are not sure if a list item applies to your research, read the appropriate section before selecting a response.

Materials & experimental systems

n/a	Involved in the study
☒	☐ Antibodies
☐	☒ Eukaryotic cell lines
☒	☐ Palaeontology
☒	☐ Animals and other organisms
☒	☐ Human research participants
☒	☐ Clinical data

Methods

n/a	Involved in the study
☒	☐ ChIP-seq
☒	☐ Flow cytometry
☒	☐ MRI-based neuroimaging

Antibodies

Antibodies used	*Describe all antibodies used in the study; as applicable, provide supplier name, catalog number, clone name, and lot number.*
Validation	*Describe the validation of each primary antibody for the species and application, noting any validation statements on the manufacturer's website, relevant citations, antibody profiles in online databases, or data provided in the manuscript.*

Eukaryotic cell lines

Policy information about cell lines

Cell line source(s)	1. African green monkey origin, Vero from ATCC; 2. African green monkey origin, Vero E6 from ATCC.
Authentication	All monkey cells were from ATCC with authentication. The authentication was performed by morphology check under microscopes and growth curve analysis.
Mycoplasma contamination	We confirm that all cells were tested as mycoplasma negative.
Commonly misidentified lines (See ICLAC register)	No commonly misidentified cell lines were used.

Palaeontology

Specimen provenance	*Provide provenance information for specimens and describe permits that were obtained for the work (including the name of the issuing authority, the date of issue, and any identifying information).*
Specimen deposition	*Indicate where the specimens have been deposited to permit free access by other researchers.*
Dating methods	*If new dates are provided, describe how they were obtained (e.g. collection, storage, sample pretreatment and measurement), where they were obtained (i.e. lab name), the calibration program and the protocol for quality assurance OR state that no new dates are provided.*

☐ Tick this box to confirm that the raw and calibrated dates are available in the paper or in Supplementary Information.

Animals and other organisms

Policy information about studies involving animals; ARRIVE guidelines recommended for reporting animal research

Laboratory animals	*For laboratory animals, report species, strain, sex and age OR state that the study did not involve laboratory animals.*
Wild animals	*Provide details on animals observed in or captured in the field; report species, sex and age where possible. Describe how animals were caught and transported and what happened to captive animals after the study (if killed, explain why and describe method; if released, say where and when) OR state that the study did not involve wild animals.*
Field-collected samples	*For laboratory work with field-collected samples, describe all relevant parameters such as housing, maintenance, temperature, photoperiod and end-of-experiment protocol OR state that the study did not involve samples collected from the field.*
Ethics oversight	*Identify the organization(s) that approved or provided guidance on the study protocol, OR state that no ethical approval or guidance was required and explain why not.*

Note that full information on the approval of the study protocol must also be provided in the manuscript.

Human research participants

Policy information about studies involving human research participants

Population characteristics	*Describe the covariate-relevant population characteristics of the human research participants (e.g. age, gender, genotypic information, past and current diagnosis and treatment categories). If you filled out the behavioural & social sciences study design questions and have nothing to add here, write "See above."*
Recruitment	*Describe how participants were recruited. Outline any potential self-selection bias or other biases that may be present and how these are likely to impact results.*
Ethics oversight	*Identify the organization(s) that approved the study protocol.*

Note that full information on the approval of the study protocol must also be provided in the manuscript.

Clinical data

Policy information about clinical studies

All manuscripts should comply with the ICMJE guidelines for publication of clinical research and a completed CONSORT checklist must be included with all submissions.

Clinical trial registration	*Provide the trial registration number from ClinicalTrials.gov or an equivalent agency.*
Study protocol	*Note where the full trial protocol can be accessed OR if not available, explain why.*
Data collection	*Describe the settings and locales of data collection, noting the time periods of recruitment and data collection.*
Outcomes	*Describe how you pre-defined primary and secondary outcome measures and how you assessed these measures.*

ChIP-seq

Data deposition

☐ Confirm that both raw and final processed data have been deposited in a public database such as GEO.

☐ Confirm that you have deposited or provided access to graph files (e.g. BED files) for the called peaks.

Data access links *May remain private before publication.*	*For "Initial submission" or "Revised version" documents, provide reviewer access links. For your "Final submission" document, provide a link to the deposited data.*
Files in database submission	*Provide a list of all files available in the database submission.*
Genome browser session (e.g. UCSC)	*Provide a link to an anonymized genome browser session for "Initial submission" and "Revised version" documents only, to enable peer review. Write "no longer applicable" for "Final submission" documents.*

Methodology

Replicates	*Describe the experimental replicates, specifying number, type and replicate agreement.*
Sequencing depth	*Describe the sequencing depth for each experiment, providing the total number of reads, uniquely mapped reads, length of reads and whether they were paired- or single-end.*
Antibodies	*Describe the antibodies used for the ChIP-seq experiments; as applicable, provide supplier name, catalog number, clone name, and lot number.*
Peak calling parameters	*Specify the command line program and parameters used for read mapping and peak calling, including the ChIP, control and index files used.*
Data quality	*Describe the methods used to ensure data quality in full detail, including how many peaks are at FDR 5% and above 5-fold enrichment.*
Software	*Describe the software used to collect and analyze the ChIP-seq data. For custom code that has been deposited into a community repository, provide accession details.*

Flow Cytometry

Plots

Confirm that:

☐ The axis labels state the marker and fluorochrome used (e.g. CD4-FITC).

☐ The axis scales are clearly visible. Include numbers along axes only for bottom left plot of group (a 'group' is an analysis of identical markers).

☐ All plots are contour plots with outliers or pseudocolor plots.

☐ A numerical value for number of cells or percentage (with statistics) is provided.

Methodology

Sample preparation	*Describe the sample preparation, detailing the biological source of the cells and any tissue processing steps used.*
Instrument	*Identify the instrument used for data collection, specifying make and model number.*
Software	*Describe the software used to collect and analyze the flow cytometry data. For custom code that has been deposited into a community repository, provide accession details.*

Cell population abundance

Describe the abundance of the relevant cell populations within post-sort fractions, providing details on the purity of the samples and how it was determined.

Gating strategy

Describe the gating strategy used for all relevant experiments, specifying the preliminary FSC/SSC gates of the starting cell population, indicating where boundaries between "positive" and "negative" staining cell populations are defined.

☐ Tick this box to confirm that a figure exemplifying the gating strategy is provided in the Supplementary Information.

Magnetic resonance imaging

Experimental design

Design type

Indicate task or resting state; event-related or block design.

Design specifications

Specify the number of blocks, trials or experimental units per session and/or subject, and specify the length of each trial or block (if trials are blocked) and interval between trials.

Behavioral performance measures

State number and/or type of variables recorded (e.g. correct button press, response time) and what statistics were used to establish that the subjects were performing the task as expected (e.g. mean, range, and/or standard deviation across subjects).

Acquisition

Imaging type(s)

Specify: functional, structural, diffusion, perfusion.

Field strength

Specify in Tesla

Sequence & imaging parameters

Specify the pulse sequence type (gradient echo, spin echo, etc.), imaging type (EPI, spiral, etc.), field of view, matrix size, slice thickness, orientation and TE/TR/flip angle.

Area of acquisition

State whether a whole brain scan was used OR define the area of acquisition, describing how the region was determined.

Diffusion MRI ☐ Used ☐ Not used

Preprocessing

Preprocessing software

Provide detail on software version and revision number and on specific parameters (model/functions, brain extraction, segmentation, smoothing kernel size, etc.).

Normalization

If data were normalized/standardized, describe the approach(es): specify linear or non-linear and define image types used for transformation OR indicate that data were not normalized and explain rationale for lack of normalization.

Normalization template

Describe the template used for normalization/transformation, specifying subject space or group standardized space (e.g. original Talairach, MNI305, ICBM152) OR indicate that the data were not normalized.

Noise and artifact removal

Describe your procedure(s) for artifact and structured noise removal, specifying motion parameters, tissue signals and physiological signals (heart rate, respiration).

Volume censoring

Define your software and/or method and criteria for volume censoring, and state the extent of such censoring.

Statistical modeling & inference

Model type and settings

Specify type (mass univariate, multivariate, RSA, predictive, etc.) and describe essential details of the model at the first and second levels (e.g. fixed, random or mixed effects; drift or auto-correlation).

Effect(s) tested

Define precise effect in terms of the task or stimulus conditions instead of psychological concepts and indicate whether ANOVA or factorial designs were used.

Specify type of analysis: ☐ Whole brain ☐ ROI-based ☐ Both

Statistic type for inference
(See Eklund et al. 2016)

Specify voxel-wise or cluster-wise and report all relevant parameters for cluster-wise methods.

Correction

Describe the type of correction and how it is obtained for multiple comparisons (e.g. FWE, FDR, permutation or Monte Carlo).

Models & analysis

n/a	Involved in the study
☐	☐ Functional and/or effective connectivity
☐	☐ Graph analysis
☐	☐ Multivariate modeling or predictive analysis

Functional and/or effective connectivity

Report the measures of dependence used and the model details (e.g. Pearson correlation, partial correlation, mutual information).

Graph analysis

Report the dependent variable and connectivity measure, specifying weighted graph or binarized graph, subject- or group-level, and the global and/or node summaries used (e.g. clustering coefficient, efficiency, etc.).

Multivariate modeling and predictive analysis

Specify independent variables, features extraction and dimension reduction, model, training and evaluation metrics.